The relation between dynamics and activity of phospholipase A/acyltransferase homologs

Chatterjee, S.D.

4

Chapter

Introduction of the PLAAT4 L2(B6) in PLAAT3 disrupts salt bridges and increases activity.

This chapter is based on joint work with Rubin Dasgupta and Juan Zhou.

The work in this chapter was published as: Chatterjee, S. D., Zhou, J., Dasgupta, R., Cramer-Blok, A., Timmer, M., van der Stelt, M., and Ubbink, M. (2021) Protein Dynamics Influence the Enzymatic Activity of Phospholipase A/Acyltransferases 3 and 4. Biochemistry 60, 1178–1190.

Abstract

NMR experiments and MD simulations provided us with insights of the differences in dynamics between PLAAT3 and PLAAT4. The rearrangement of L2(B6) loop was found unique to PLAAT4 which prompted us to observe the significance of the loop. Site directed mutagenesis followed by phospholipase assay revealed that swapping of loop L2(B6) in PLAAT3 and PLAAT4 bring about significant increase in activity. On the basis of molecular dynamics simulations, we speculate that this increase in activity is due to the disruption of existing salt bridges in the wild type proteins, thereby rendering the loop-mutants more flexible in order for better substrate accessibility and accommodation as revealed by salt-bridge lifetime analysis.

Introduction

Observations reported in Chapters 2 and 3 provided us with significant insights into the distinct dynamic profiles of the soluble domains of PLAAT3 and PLAAT4. The two proteins differ in the number and dispersion of salt bridges, which is a likely cause for the difference in melting temperature. NMR experiments and MD simulations provided evidence for large differences in dynamics. An interesting rearrangement of loop L2(B6) unique to PLAAT4 was seen, making its active site region more mobile than that of PLAAT3. The main research question being why the two proteins differ in activity, despite sharing similar sequence and structure, we wondered whether the dynamics of loop L2(B6) plays a role in the activity difference. This hypothesis was tested by swapping the L2(B6) region of PLAAT3 and PLAAT4 and studying the effects using *in vitro* activity tests and MD calculations. According to the hypothesis, a gain-of-function in the PLAAT3 variant with the L2(B6) region of PLAAT4 was expected, whereas for PLAAT4 with the L2(B6) region of PLAAT3 the opposite was foreseen.

Results

To probe whether the mobility of L2(B6) contributes to the activity of PLAAT4, mutagenesis was performed, both *in silico* and *in vitro*. Wild type PLAAT3 and PLAAT4 were mutated by swapping their L2(B6) loop (residues 103-111) *in vitro* to test whether L2(B6) is critical for conferring enhanced dynamics in PLAAT4 (Figure 4.1). The mutants were named PLAAT3_L2(B6)$_4$ and PLAAT4_L2(B6)$_3$ to indicate the mutants of PLAAT3(4) with the L2(B6) region from PLAAT4(3). Phospholipase assay was performed to establish the functional effects of the mutagenesis. The dynamics of the mutants were probed by MD simulations.

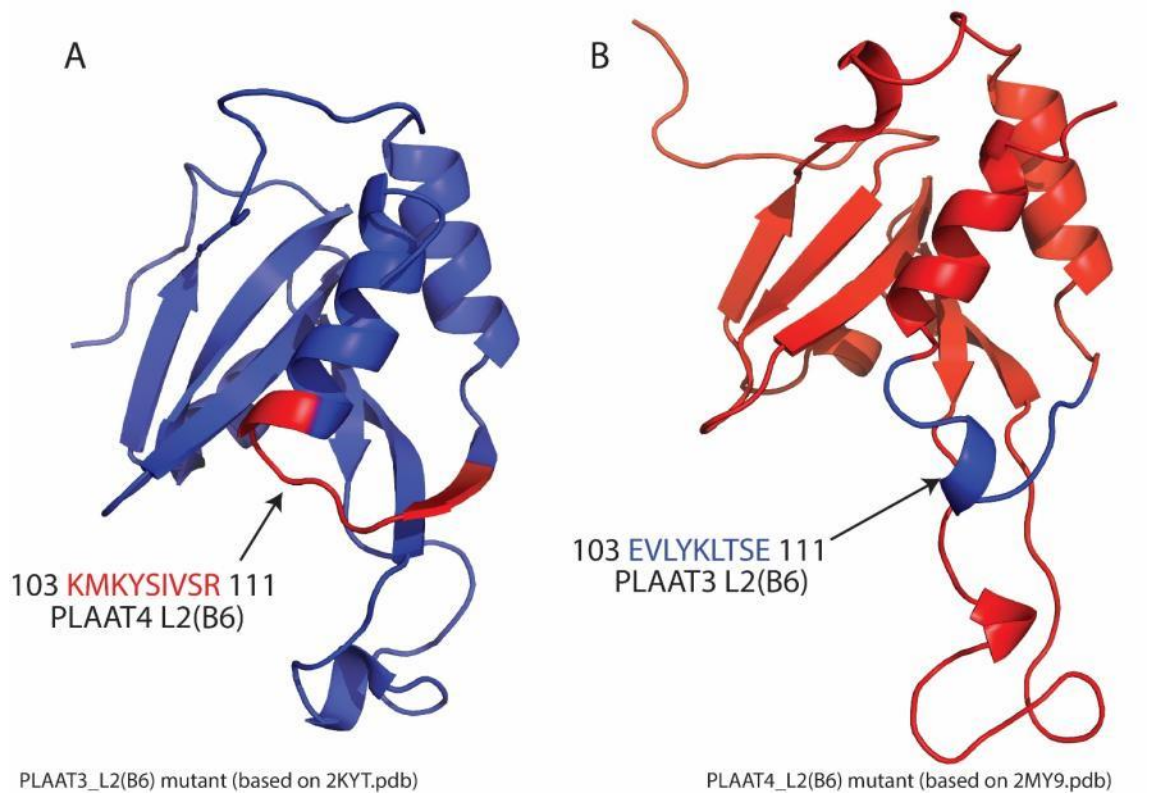

Figure 4.1 Models of mutants of PLAAT3-L2(B6)$_4$ (A) and PLAAT4-L2(B6)$_3$ (B). The mutated regions are shown in contrasting colors.

Phospholipase assay. A phospholipase assay with the fluorescent substrate Red/Green BODIPY^{TM} PC-A2 was performed to check the activity of both wild type and mutant proteins. The assay releases the green fluorescent fatty acid BODIPY^{TM} FL C5 from the *sn*-2 position of the substrate. The reaction rate (expressed in pmol/min/mg protein) of each protein is plotted in Figure 4.2. The results show that the reaction rate of wild type PLAAT4 was high, whereas wild type PLAAT3 has background activity. Interestingly, PLAAT3_L2(B6) shows a large

increase in the reaction rate. This observation suggests that either the natural L2(B6) in PLAAT3 was inhibiting the activity or that PLAAT4 L2(B6) enables activity. When the PLAAT4 L2(B6) was replaced with the analogous loop of PLAAT3, a small increase in activity was seen, as compared to wild type PLAAT4. Thus, replacement of $L2(B6)_3$ with $L2(B6)_4$ in PLAAT3 enables activity, whereas the opposite mutation does not inhibit activity in PLAAT4.

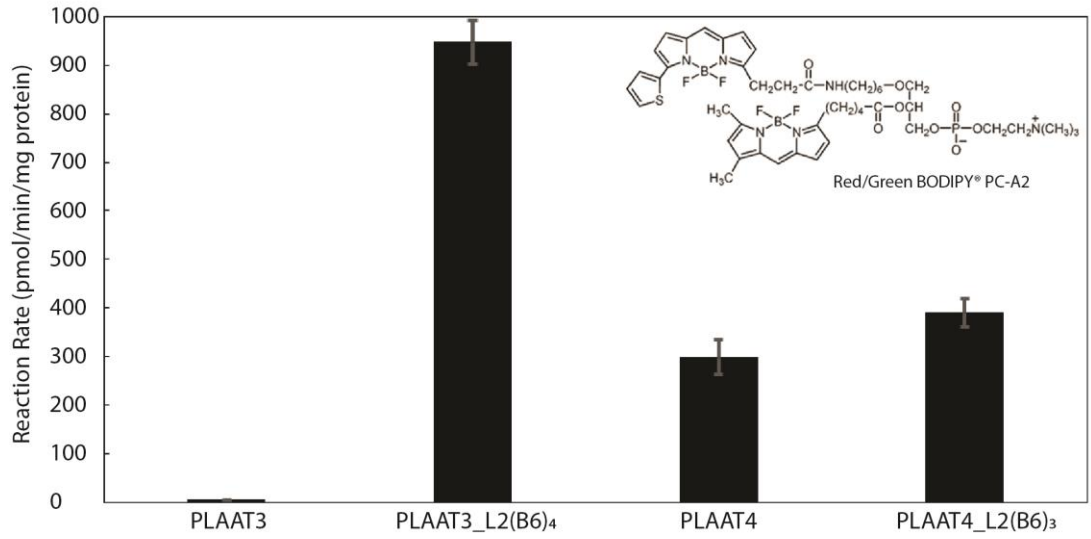

Figure 4.2 Phospholipase assay with Red/Green BODIPY® PC-A2 (inset). The activity towards Red/Green Bidopy PC-A2 is plotted for PLAAT wild type and loop mutants.

Conformational freedom in the mutants. Molecular dynamics (MD) simulations were performed to sample the trajectories for both the wild type and the L2(B6) mutants for 100 ns. Two seeds starting the simulation at different points in the energy landscape were used. The first model of each of the published NMR structures [1,2] was used as starting structure for the wild type proteins, whereas the starting structures for the mutants were generated by in silico mutagenesis (Materials and Methods). The fluctuations during the MD runs were visualized by plotting the all-atom RMSD of the L2(B6) as a function of the runtime. The results for the mutants were compared with the corresponding wild type proteins. Insertion of $L2(B6)_4$ did not significantly alter the overall RMSD of PLAAT3. The RMSD stabilizes around 2.5 Å (Figure 4.3.A). Similarly, the PLAAT4-$L2(B6)_3$ mutant displays an RMSD trajectory that resembles that of wild type PLAAT4. Wild type and mutant PLAAT4 proteins exhibit larger

RMSD (~ 4.5 Å) than PLAAT3, indicating that PLAAT4 samples a larger structural space than PLAAT3 (Figure 4.3.B).

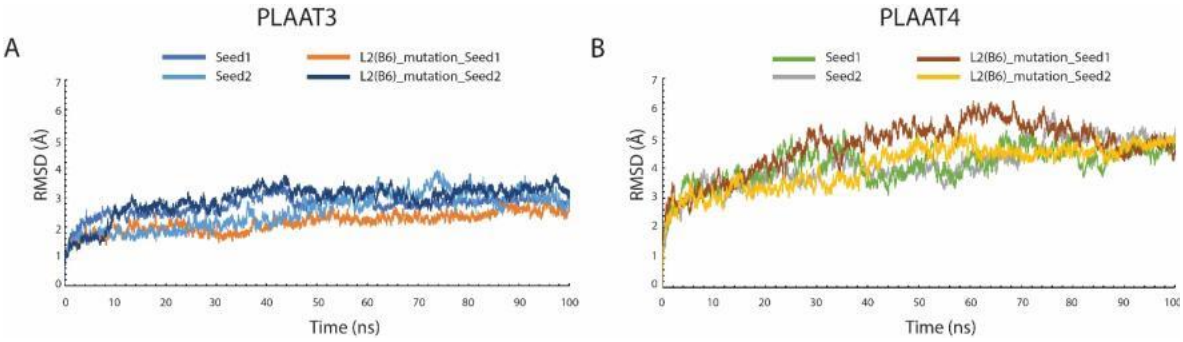

Figure 4.3 Structural fluctuations on the nanosecond timescale. All-atom RMSD values of wild type and L2(B6) swapped mutants during 100 ns MD runs are plotted for PLAAT3 (A) and PLAAT4 (B). The data represent structure snapshots saved at every ps of the trajectory.

Since the overall RMSD is strongly influenced by the presence of the highly dynamic loop L1, the RMSD of the L2(B6) loop alone in both wild type and mutant proteins as a function of the runtime was also analysed (Figure 4.4). Interestingly, substitution of $L2(B6)_3$ with $L2(B6)_4$ did not significantly increase the conformational freedom of the loop in PLAAT3 (Figure 4.4A). Analogously, in PLAAT4 the large motions of the loop in the wild type protein are not reduced by introduction of $L2(B6)_3$. The motions rather appear to be enhanced somewhat (Figure 4.4B).

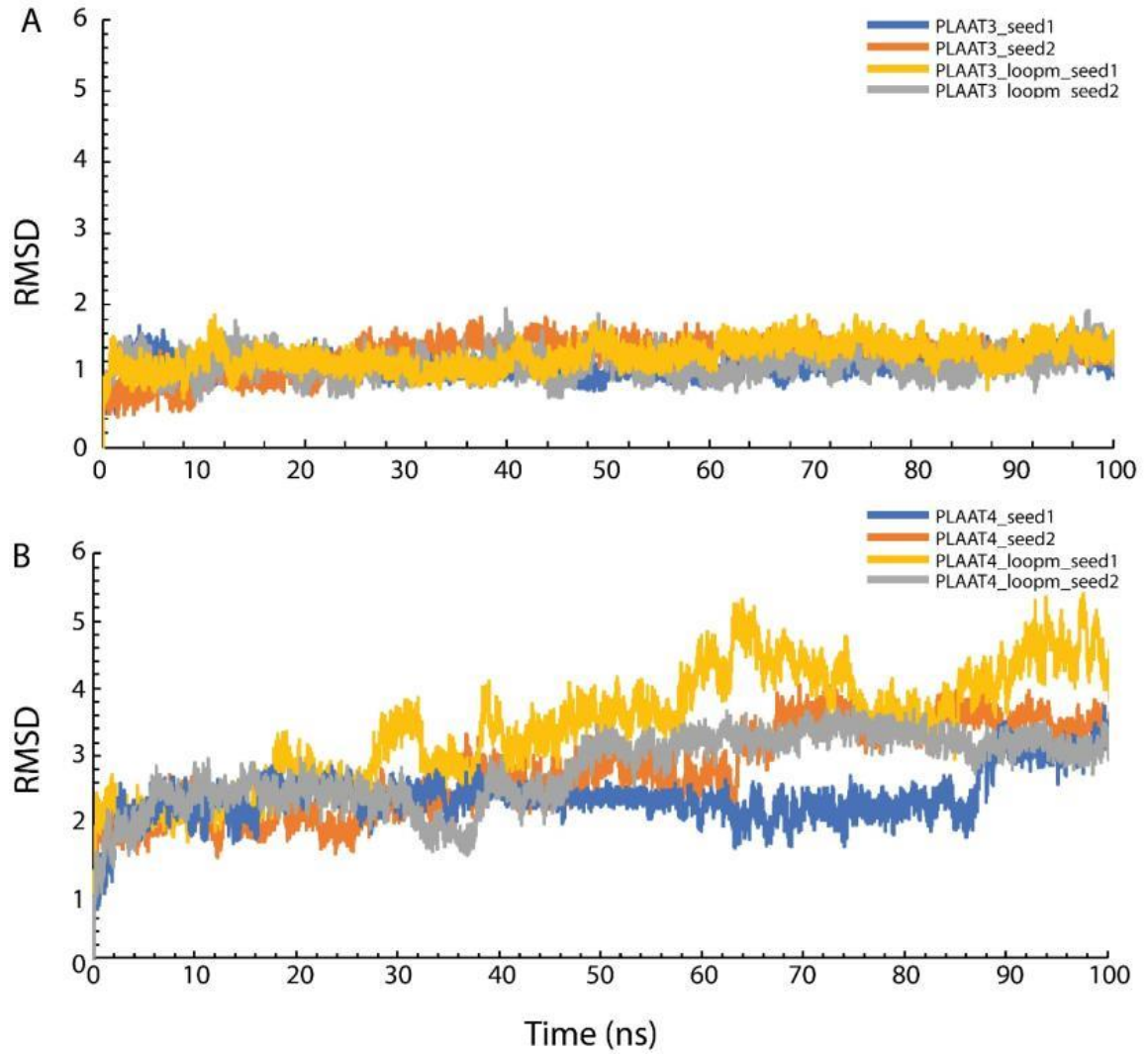

Figure 4.4. L2(B6) loop motions. The RMSD values of the L2(B6) loops of PLAAT3 (A) and PLAAT4 (B) in wild type and mutant proteins are plotted against the MD simulation time. The data represent structure snapshots saved at every ps of the trajectory. "loopm" in the legend refers to L2(B6) mutant.

To test for the presence of larger, correlated motions that influence the accessibility of the active site, the variation of the length of two vectors connecting distance parts of the proteins was analysed. The first vector runs along the His residues of the catalytic triad and connects the Cα atoms of residues R22 and K62, which are located in different strands of the twisted β-sheet. The second vector is oriented roughly perpendicular, going across the active site and connecting the Cα atoms of residues V68 (α-helix A1) and C113, the active site cysteine residue (α-helix A3), see Figure 4.5. In the MD runs of both wild type and mutant PLAAT3, the length of vector 1 is stable at 18 Å, with rapid fluctuations of about 1 Å, indicating a lack of correlated

motions along this vector over the time of the simulation. For the wild type PLAAT3 the vector connecting V68 and C113 is also stable at 13-14 Å, after initial equilibration during the first 10-15 ns. For PLAAT3_L2(B6)$_4$ the vector shows more variation with a large excursion to 18 Å for about 10 ns in one of the runs and shorter excursions to increased length in the other run (Figure 4.5). This could be an indication that PLAAT3_L2(B6)$_4$ undergoes relatively slow, correlated motions that affect the active site. For PLAAT4, a similar analysis shows that also here vector 1 has a stable length over the time of the simulation. Vector 2 shows large excursions with prolonged lifetimes, similar to PLAAT3_L2(B6)$_4$, for both the wild type PLAAT4 and PLAAT4_L2(B6)$_3$ (Figure 4.6).

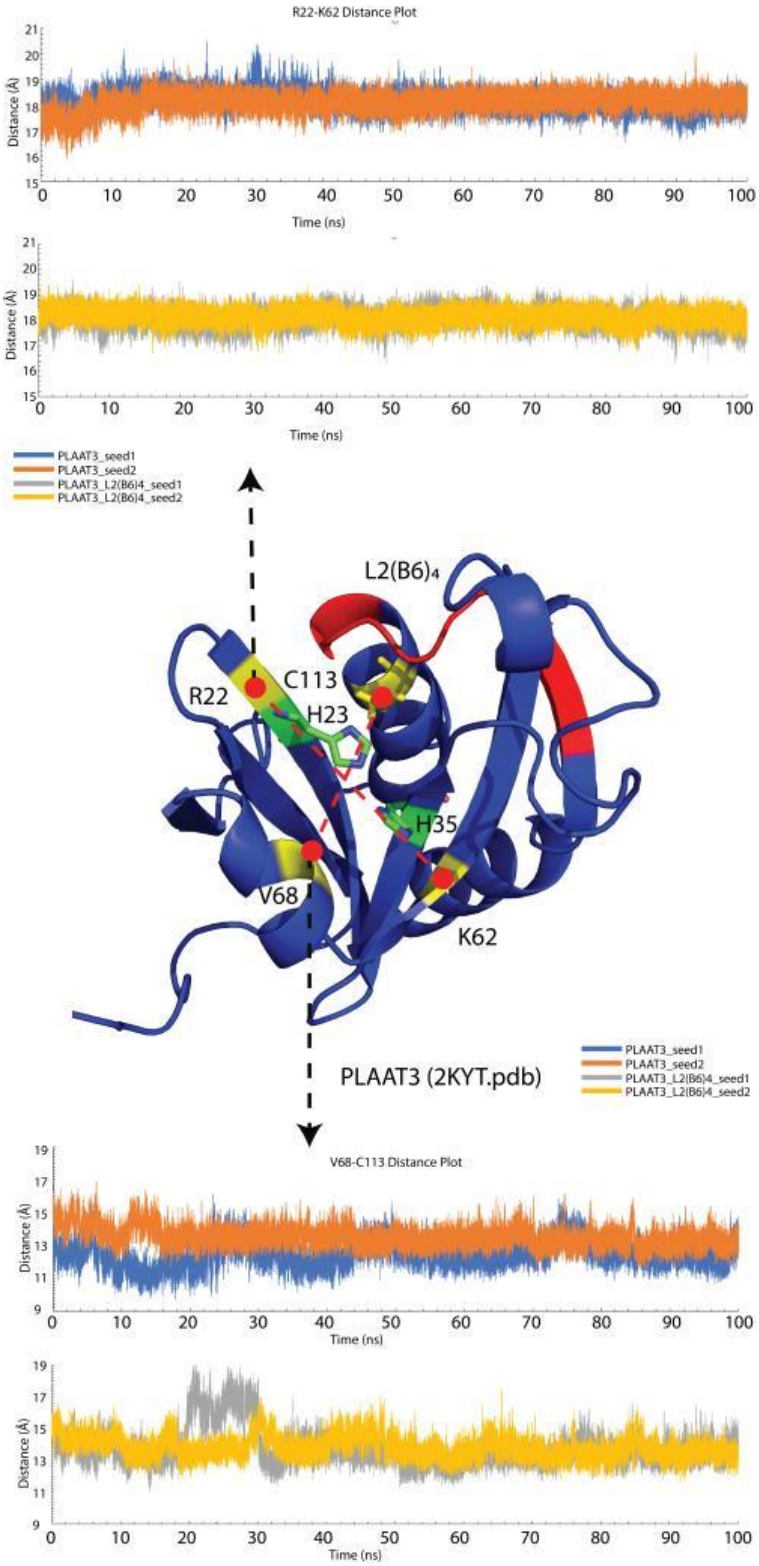

Figure 4.5. Correlated motions across the active site. Vectors 1 and 2 connect the Cα atoms of R22 & K62, and V68 & C113, respectively, and are indicated with red dashed lines in the structure of PLAAT3 (PDB 2KYT, [2]) with $L2(B6)_4$ modelled in. The active site residues H23, H35 and C113 are depicted as sticks. The plots above (vector 1) and below (vector 2) show the vector length during MD runs of wild type and mutant PLAAT3.

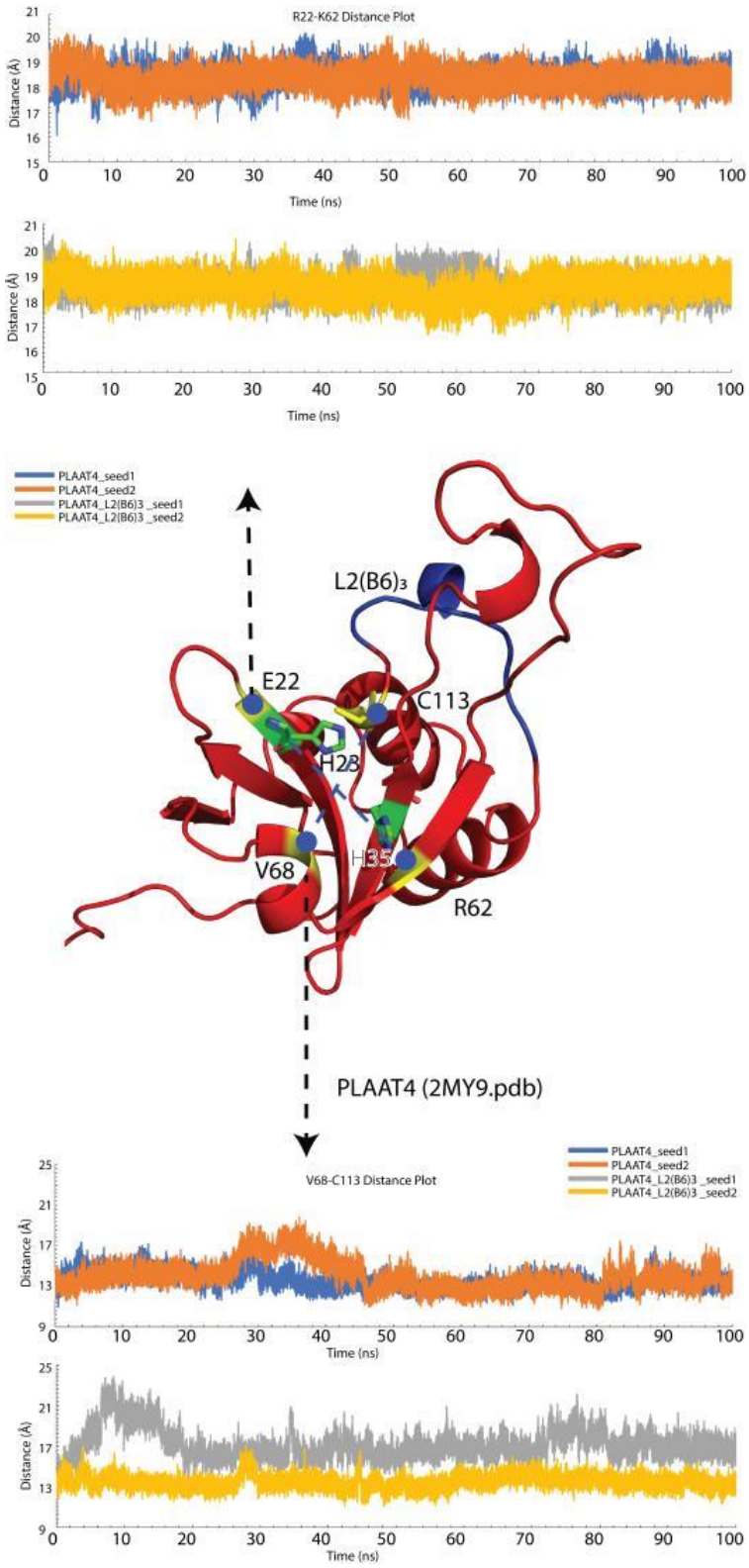

Figure 4.6. Correlated motions across the active site. Vectors 1 and 2 connect the Cα atoms of R22 & K62, and V68 & C113, respectively, and are indicated with red dashed lines in the structure of PLAAT4 (PDB 2MY9, [1]) with $L2(B6)_3$ modelled in. The active site residues H23, H35 and C113 are depicted as sticks. The plots above (vector 1) and below (vector 2) show the vector length during MD runs of wild type and mutant PLAAT4.

Salt-bridges. Another measure of structural integrity is the presence of salt bridges during the MD run. For regions that sample the same conformations in wild type and mutant forms of the protein, it is expected that salt bridges are formed during the same fraction of the time. The presence of salt bridges was sampled every 10 ps over the entire MD trajectory and considered significant if the interaction was present on average over two runs for at least 20% of the time. Surprisingly large differences were found between wild type and loop mutants. In wild type PLAAT3, 11 salt bridges were identified (Table 4.1, Figure 4.7), whereas in PLAAT3_L2(B6)$_4$ only five of these remained. The lost interactions involved residues in the L2B6 loop but also across the active site and even at the other end of the protein. Residues that lose the bridges found in the wild type protein form new ones with other charged residues. A similar picture arises from the data of PLAAT4. Out of seven salt-bridges in wild type PLAAT4, only three were found in PLAAT4_L2(B6)$_3$ (Table 4.2, Figure 4.7). The lost bridges are in the loop, the active site and around D81, at the other end of the protein. Only one new salt-bridge was found in PLAAT4_L2(B6)$_3$. It is concluded that, despite the lack of changes in the overall and loop RMSD, the average structures clearly differ in details between wild type and loop mutants.

Table 4.1. Salt bridges in PLAAT3. The populations of salt bridges (in %) in PLAAT3 and PLAAT3_L2(B6)$_4$ during 100 ns MD runs are reported for two runs (Seeds 1 and 2). Average populations of ≥ 20% are considered significant. Interactions that are insignificant are shown underlined. Salt bridges absent in wild type PLAAT3 but observed in PLAAT3_L2(B6)$_4$ are demarcated by a solid line (salt bridges in 12-14).

Populations (%)							
	Salt Bridges	**WT Seed 1**	**WT Seed 2**	**Average**	**L2(B6)$_4$ Seed 1**	**L2(B6)$_4$ Seed 2**	**Average**
1	ASP12--LYS9	29	20	24.5	12	33	22.5
2	ASP67--ARG2	10	31	20.5	5	0	2.5
3	ASP72--ARG18	24	39	31.5	35	5	20
4	ASP81--ARG121	3	80	41.5	0	0	0
5	ASP82--LYS83	29	25	27	0	8	4
6	GLU103--LYS57	34	42	38	0	0	0
7	GLU114--LYS79	13	33	23	32	20	26
8	GLU15--ARG22	23	31	27	24	4	14
9	GLU41--LYS61	53	54	53.5	17	1	9
10	GLU63--HIS35	44	39	41.5	35	35	35
11	GLU97--LYS62	43	43	43	51	47	49
12	ASP12--ARG121	0	0	0	75	6	40.5
13	ASP56--LYS57	4	2	3	34	27	30.5
14	GLU119--HIS115	0	6	3	0	29	14.5
15	GLU98--ARG95	0	1	0.5	11	43	27

Table 4.2. Salt bridges in PLAAT4. The populations of salt bridges (in %) in PLAAT4 and PLAAT4_L2(B6)$_3$ during 100 ns MD runs are reported for two runs (Seeds 1 and 2). Average populations of ≥ 20% are considered significant. Interactions that are insignificant are shown in underlined. Salt bridges absent in wild type PLAAT4 but observed in PLAAT4_L2(B6)$_3$ are demarcated by a solid line (salt bridge in 8).

Populations (%)							
	Salt Bridges	**Seed 1**	**Seed 2**	**Average**	**L2(B6)$_3$ Seed 1**	**L2(B6)$_3$ Seed 2**	**Average**
1	ASP12--LYS9	25	43	34	43	33	38
2	ASP67--ARG64	35	32	33.5	23	42	32.5
3	ASP81--ARG121	36	49	42.5	0	17	8.5
4	GLU114--ARG111	39	46	42.5	0	0	0
5	GLU15--ARG75	19	35	27	49	66	57.5
6	GLU22--ARG111	37	17	27	0	0	0
7	GLU59--LYS103	31	28	29.5	0	0	0
8	GLU111--HIS23	0	0	0	0	32	16

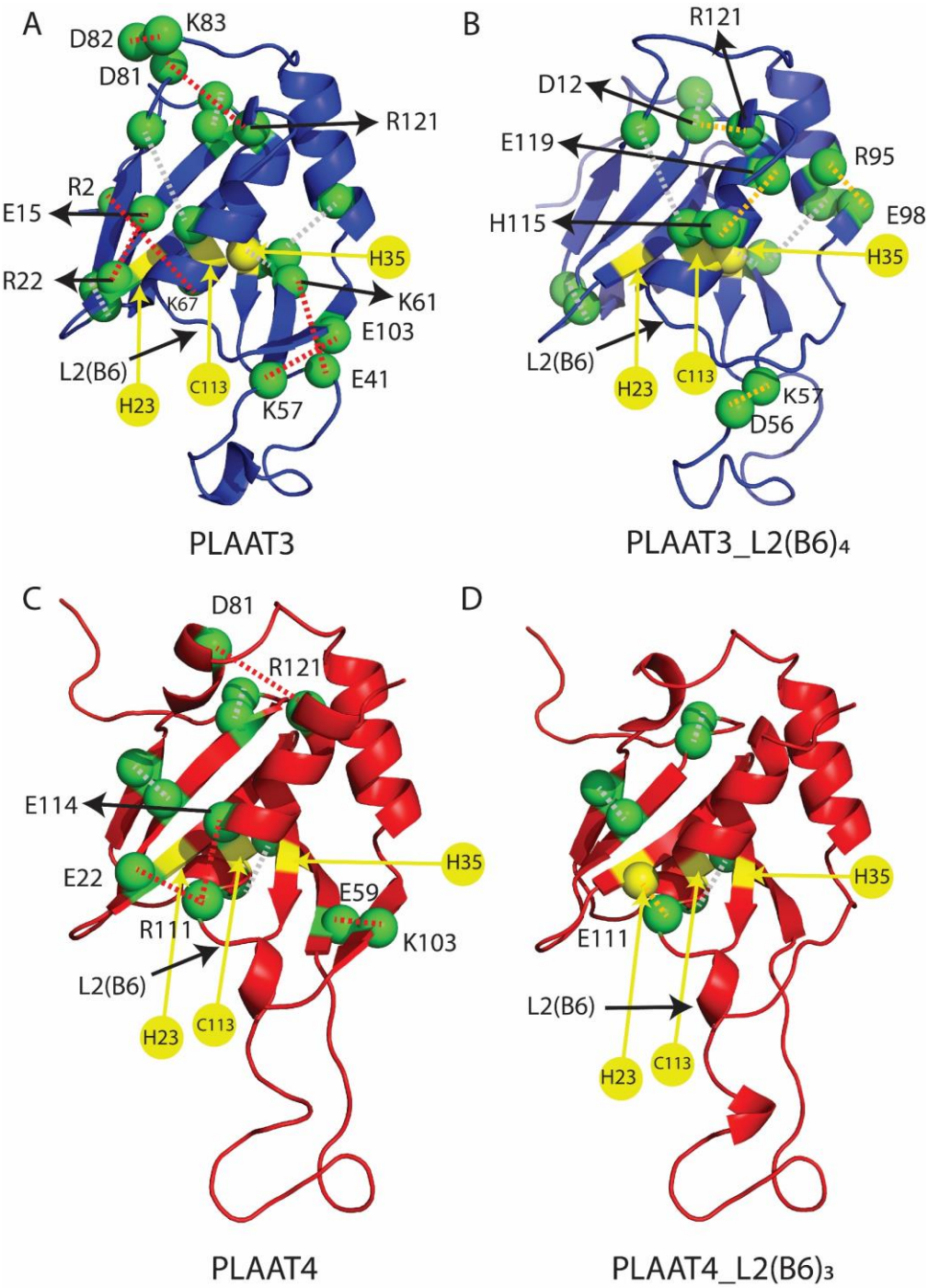

Figure 4.7 Salt bridges in wild type and loop mutant PLAAT proteins. Residues involved in salt bridges with a combined average lifetime of at least 20% in the two 100 ns MD runs are shown with green spheres for Cα atoms. Dashed lines indicate the presence of salt bridges between the side chains of the connected residues, in wild type only (red), wild type and mutant (grey) or mutant only (yellow), for PLAAT3 (A), PLAAT3_L2(B6)$_4$ (B), PLAAT4 (C) and PLAAT4_L2(B6)$_3$ (D). The residues of the catalytic triad are marked in yellow.

Discussion

While further investigating the cause of differences in PLAAT3/4 phospholipase activity, we gathered interesting observations from the last two chapters on whose basis, we formed a hypothesis. We found that PLAAT4 is inherently more dynamic than PLAAT3 due to less salt bridges and that residues around the PLAAT4 active site might have more solvent accessibility, due to L2(B6) mobility. In this chapter we performed experiments and simulations to test our hypothesis.

The phospholipase assay showed that wild type PLAAT4 has a higher reaction rate compared to wild type PLAAT3, which is in agreement with the literature [3]. Furthermore, by changing the loop region of PLAAT3 for the loop region of PLAAT4 the activity increases compared to wild type PLAAT3. This strongly indicated that the L2(B6) mutation in PLAAT3 introduced greater dynamics around the active site region causing increased substrate accessibility. However, when PLAAT3 L2(B6) was introduced in PLAAT4, the activity increased as well. Therefore, it can be concluded that the loop region alone does not determine the activity, but it does have a large effect on the activity.

We performed in-silico mutagenesis by swapping the L2(B6) between PLAAT3 and PLAAT4 and performed two runs of MD simulations for 100 ns, followed by an analysis of salt-bridge lifetimes during the MD simulations. We found that the RMSD profiles of PLAAT3 and PLAAT3_L2(B6) were similar, while the RMSD profiles of PLAAT4 and PLAAT4_L2(B6), although distinct in the middle of an MD run, converged at the end of the runs suggesting that the PLAAT4 and PLAAT4_L2(B6) are not very different with respect to conformation. Furthermore, the study of concerted motions of the two opposite vectors involving R22-K62 and V68-C113 residue pairs also did not yield clear differences in dynamics between the wild-type and mutant proteins. As discussed in Chapter 2, PLAAT3 has a well-dispersed network of salt bridges, so the effect of PLAAT4 L2(B6) introduction on the existing salt bridges was analyzed.

Salt bridge life-time analysis revealed that introduction of PLAAT4 L2(B6) in PLAAT3 caused disappearance of 50% existing salt bridges, while adding 5 more in different parts of the structure. The existing salt bridge in the wild type PLAAT3 L2(B6) disappeared in the mutant, allowing its movement. This mobility due to lack of salt bridges might be crucial for greater

solvent accessibility. A similar effect was observed in PLAAT4_L2(B6)$_3$, which caused disappearance of 50% existing salt bridges in PLAAT4 suggesting that the swapping of L2(B6) changes the chemical environment and existing salt bridge networks in both PLAAT3 and PLAAT4. This observation, along with the data from phospholipase assay, strongly support our hypothesis that the L2(B6) mutation in PLAAT3 restructured the salt bridges and introduced greater dynamics around the active site region, causing increased substrate accessibility. Further analysis on the structure is needed to determine how these loop residues alter the activities.

Materials and Methods

Mutagenesis. Fragment-based mutagenesis[4] was carried out by forward and reverse primers (final concentration of 12µM) designed to swap the L2(B6) loop of PLAAT3 (103E-V-L-Y-K-L-T-S-E111) with that of PLAAT4 (103K-M-K-Y-S-I-V-S-R111) and vice versa. PCR amplification of the two fragments were performed by a cycle of the following temperature steps- 95°C for 10 minutes followed by 25 cycles of 95°C for 30 seconds, 55°C for 30 seconds, 68°C for 1 minute followed by termination of the reaction at 68°C for 10 minutes. The amplified fragments obtained thereby were purified (GFX^{TM} PCR DNA purification Kit, GE Healthcare) and combined using a second similar PCR step before subcloning into E. coli KA797 cells using the common NcoI and XhoI restriction sites in the PLAAT genes.

Protein Production and Purification. DNA sequences encoding the human N-terminal soluble form (residues 1–125) of PLAAT3 or PLAAT4 (Uniprot ID P53816 and Q9UL19, respectively) with N-terminal His$_6$ tag and a TEV cleavage site were ordered from GeneArt. The fragments were inserted in-frame into bacterial expression vector pET-28a using the *Nco*I and *Xho*I restriction sites. Chemically competent *Escherichia coli* BL21-DE3pLys cells were transformed with the plasmids for protein production. The bacteria were cultured overnight in 50 mL of LB medium with 50 µg/mL kanamycin at 37^{o}C under shaking. 5 mL of the overnight pre-culture was transferred to 500 mL LB medium with 50 µg/mL kanamycin. When the OD_{600} reached 0.6, the temperature was lowered to 22^{o}C and gene expression was induced by addition of 0.5 mM IPTG. The culture was incubated for 5 hours before cells were harvested by centrifugation at 6000 rpm at 4^{o}C. The pellet was resuspended in 5 mL of 50 mM Tris–HCl buffer (pH 7.5) followed by freezing at -80^{o}C overnight. The cells were thawed the next day in presence of DNase I and lysozyme and lysed by French press. The lysate was centrifuged at

4°C at 25000g for 45 min. The supernatant of the cell lysate containing the His_6-tagged soluble protein was then loaded on a HiTrap-Nickel column, equilibrated with 50 mM Tris pH 7.5, 500 mM NaCl and 5 mM Imidazole. The protein was eluted using a linear imidazole concentration gradient from 0 to 0.5 M. The collected fractions were pooled and dialyzed overnight using a 3.5 kDa molecular weight cut-off cellulose membrane at 4°C in 50 mM Tris, pH 7.5, 500 mM NaCl, 0.5mM EDTA buffer to remove imidazole. His_6-tagged TEV protease was added for the cleavage of the His_6-tag on PLAAT during dialysis overnight. The mixture was loaded again on a His_6-Trap Nickel column to collect the N-terminal PLAAT3 and PLAAT4 domains. The buffer was changed into 50 mM Tris-HCl, 50 mM NaCl, 10 mM DTT, pH 7.5. The volume of the sample was reduced to 2.5 mL using a 5 kDa MWCO Amicon Ultracentrifugal filter (EMD Millipore) at 2200 g and 15 °C. The concentrated sample was loaded on and eluted from a Superose12 gel filtration column in 30 mM sodium phosphate buffer with 30 mM NaCl and 10 mM DTT at pH 7.0.

Phospholipase assay. [These assays were performed by Juan Zhou.] Protein solutions (200 µL, 0.1 mg/mL) were diluted with equal volume of buffer A (50 mM Tris-HCl, pH 8, 50 mM NaCl, 2 mM DTT). These solutions were added to white 96-well plates (60 µL per well, in triplicate). A standard dilution series of the product BODIPY™ PC-A2 (ThermoFischer Scientific) was prepared in pure DMSO of the following concentrations: 0.0 µM (pure DMSO), 0.005 µM, 0.01 µM, 0.05 µM, 0.1 µM, 0.5 µM, 1 µM. The product was diluted with a 1:1 mixture of buffer A and buffer B (50 mM Tris-HCl pH 8, 100 mM NaCl, 1 mM $CaCl_2$). The solutions of standards were added in the 96-well plate (100 µL each). The liposome mixture was prepared by mixing DOPC (5.1 µL, 10 mM stock in ethanol), DOPG (5.1 µL, 10 mM stock in ethanol) and the substrate Red/Green BODIPY™ PC-A2 dissolved in pure DMSO (5.1 µL, 1.5 mM, ThermoFischer Scientific). The mixture was injected slowly (in about 45 sec.), under vortexing, into a glass vial containing 1.5 mL assay buffer, using a pipette fitted with a narrow orifice gel-loading tip. The liposome mixture (50 µL) was added to each well of the 96-well plate in which the enzymes were to be tested. Then, PLAAT protein solutions (50 µL) were transferred from the white 96-well plate to the black microplate wells containing the liposome mixture at 37 °C. The fluorescence measurement was started immediately, every 20 seconds in 60 minutes on a Tecan GENios with a gain of about 54 and an excitation filter at 488 nm and emission filter at 530/590 nm.

In-silico mutagenesis. L2(B6) loops were swapped between PLAAT3 and PLAAT4 by mutating the wild type NMR structures with Chimera [5] and selecting the most favourable conformation for each mutated residue. Clashes were removed during energy minimisation in Gromacs [6].

MD simulations. MD simulations were performed using Gromacs-5.1.[67] The NMR structure of PLAAT3 (2KYT) [2], PLAAT4 (2MY9) [1] and the corresponding derived structures from *in-silico* mutagenesis were taken as starting structures and to create topology files. The AMBER ff99sb-ILDN force-field provided with GROMACS was used.[8] The models were then solvated in a periodic water box of 1 nm and 2 nm cubic edge length for PLAAT3 and PLAAT4, respectively. The latter is larger due to the elongated conformation of the protein. The TIP3Pwater model was used.[9,10] Three Na^+ counter ions were automatically placed by the GROMACS program throughout the water box such that the final system had net zero charge. After solvation and neutralization, the systems were energy minimized by 5000 steps of minimization using the steepest descent algorithm. Minimized systems were further equilibrated under NVT and NPT conditions for 500 ps with a step size of 2 fs using position restraints on the protein and a temperature of 300 K and 1 atm. pressure, controlled by the velocity rescaling (modified Berendsen) thermostat [11] and Parrinello-Rahman barostat.[12] The equilibrated systems were subjected to a 100 ns simulation run under NPT without any position restraints, and coordinates were saved after every ps. Two simulations were carried out with different starting seeds, where each seed represents a simulation at a different velocity. The trajectories were analysed using the inbuilt modules available in the GROMACS suite and visualized by means of the VMD[13]/Chimera[5] program.

Salt-bridge analysis. Salt bridge populations were calculated using VMD[13] by sampling a structure every 10 ps. The data were extracted and analysed using an in-house written python program. Only residue-pairs with salt bridges having populations of 20% or more, averaged over both runs, were taken into consideration.

References

(1) Wei, H., Wang, L., Ren, X., Yu, W., Lin, J., Jin, C., and Xia, B. (2015) Structural and functional characterization of tumor suppressors TIG3 and H-REV107. *FEBS Lett. 589*, 1179–1186.

(2) Ren, X., Lin, J., Jin, C., and Xia, B. (2010) Solution structure of the N-terminal catalytic domain of human H-REV107--a novel circular permutated NlpC/P60 domain. *FEBS Lett. 584*, 4222–4226.

(3) Golczak, M., Kiser, P. D., Sears, A. E., Lodowski, D. T., Blaner, W. S., and Palczewski, K. (2012) Structural basis for the acyltransferase activity of lecithin:retinol acyltransferase-like proteins. *J. Biol. Chem. 287*, 23790–23807.

(4) Heydenreich, F. M., Miljuš, T., Jaussi, R., Benoit, R., Milić, D., and Veprintsev, D. B. (2017) High-throughput mutagenesis using a two-fragment PCR approach. *Sci. Rep. 7*, 6787.

(5) Pettersen, E. F., Goddard, T. D., Huang, C. C., Couch, G. S., Greenblatt, D. M., Meng, E. C., and Ferrin, T. E. (2004) UCSF Chimera—A visualization system for exploratory research and analysis. *J. Comput. Chem. 25*, 1605–1612.

(6) Van Der Spoel, D., Lindahl, E., Hess, B., Groenhof, G., Mark, A. E., and Berendsen, H. J. C. (2005) GROMACS: Fast, flexible, and free. *J. Comput. Chem. 26*, 1701–1718.

(7) Hess, B., Kutzner, C., van der Spoel, D., and Lindahl, E. (2008) GROMACS 4: algorithms for highly efficient, load-balanced, and scalable molecular simulation. *J. Chem. Theory Comput. 4*, 435–447.

(8) Lindorff-Larsen, K., Piana, S., Palmo, K., Maragakis, P., Klepeis, J. L., Dror, R. O., and Shaw, D. E. (2010) Improved side-chain torsion potentials for the Amber ff99SB protein force field. *Proteins 78*, 1950–1958.

(9) Jorgensen, W. L. (1981) Quantum and statistical mechanical studies of liquids. 10. Transferable intermolecular potential functions for water, alcohols, and ethers. Application to liquid water. *J. Am. Chem. Soc. 103*, 335–340.

(10) Mark, P., and Nilsson, L. (2001) Structure and dynamics of the TIP3P, SPC, and SPC/E water models at 298 K. *J. Phys. Chem. A 105*, 9954–9960.

(11) Bussi, G., Donadio, D., and Parrinello, M. (2007) Canonical sampling through velocity rescaling. *J. Chem. Phys. 126*, 14101.

(12) Parrinello, M., and Rahman, A. (1981) Polymorphic transitions in single crystals: A new molecular dynamics method. *J. Appl. Phys. 52*, 7182–7190.

(13) Humphrey, W., Dalke, A., and Schulten, K. (1996) VMD: Visual molecular dynamics. *J.*

Mol. Graph. 14, 33–38.